An introduction to scanning transmission electron microscopy for parasitology samples

Sylvain Trépout[1], Marie-Laure Sgarra[2], Sergio Marco[2], and Georg Ramm[1]

[1]Monash University Monash Biomedicine Discovery Institute
[2]Sanofi

August 2, 2023

Abstract

Since its inception in the 1930's, transmission electron microscopy (TEM) has been a powerful method to explore the cellular structure of parasites. TEM usually requires samples of < 100 nm thick and with parasites being larger than 1 µm, their study requires resin embedding and ultrathin sectioning. During the past decade, several new methods have been developed to improve, facilitate and speed-up the structural characterisation of biological samples, offering new imaging modalities for parasitology. In particular, scanning transmission electron microscopy (STEM) can be used to observe sample sections as thick as 1 µm thus becoming an alternative to conventional TEM. STEM can also be performed under cryogenic conditions in combination with cryo-electron tomography providing access to the study of thicker samples in their native hydrated states in 3D. This method, called cryo-scanning transmission electron tomography (cryo-STET), was first developed in 2014. This review presents the basic concepts and benefits of the STEM methods and provides examples to illustrate the potential for new insights into the structure and ultrastructure of parasites.

Introduction

Parasitology studies parasites and their interactions with their natural hosts. Parasites are diverse and range from unicellular to multicellular organisms. The size of parasites can vary between micrometres for unicellular parasites up to several millimetres or even centimetres for multicellular organisms. A recent review shows how different imaging modalities (light, X-ray, electron and ion microscopies) can be used to study parasites[1]. The highest resolution structural studies of parasites are usually performed using electron microscopy. For transmission electron microscopy, parasites are thick samples and cannot be studied as is, they must be thinned down. This is classically performed by conventional EM on dehydrated resin embedded samples (Fig. 1, top-left) which consists of different sample preparation steps:

1. fixation with paraformaldehyde and glutaraldehyde
2. staining with osmium tetroxide (also acts as a fixative agent) and heavy metals (e.g. uranyl acetate)
3. dehydration in ethanol (and acetone)
4. embedding the sample in a resin which can be solidified using heat or UV-light

This eventually creates a solid block of sample that must be cut into thin sections using a diamond knife in an ultramicrotome (Fig. 1, bottom-left). Then, the sections can be observed at the electron microscope using TEM. Conventional TEM is an extremely useful method to study the ultrastructure of cells and organisms as it allows tracking membrane and organelle contours permitting to identify cell compartments. Resin blocks can be stored for several years and sections deposited on EM grids can be re-imaged several times if required. For decades, the structure of parasites has been explored using conventional TEM[2]. These studies allowed describing the internal organisation of the cells and helped with the phylogenetic classification of parasite species.

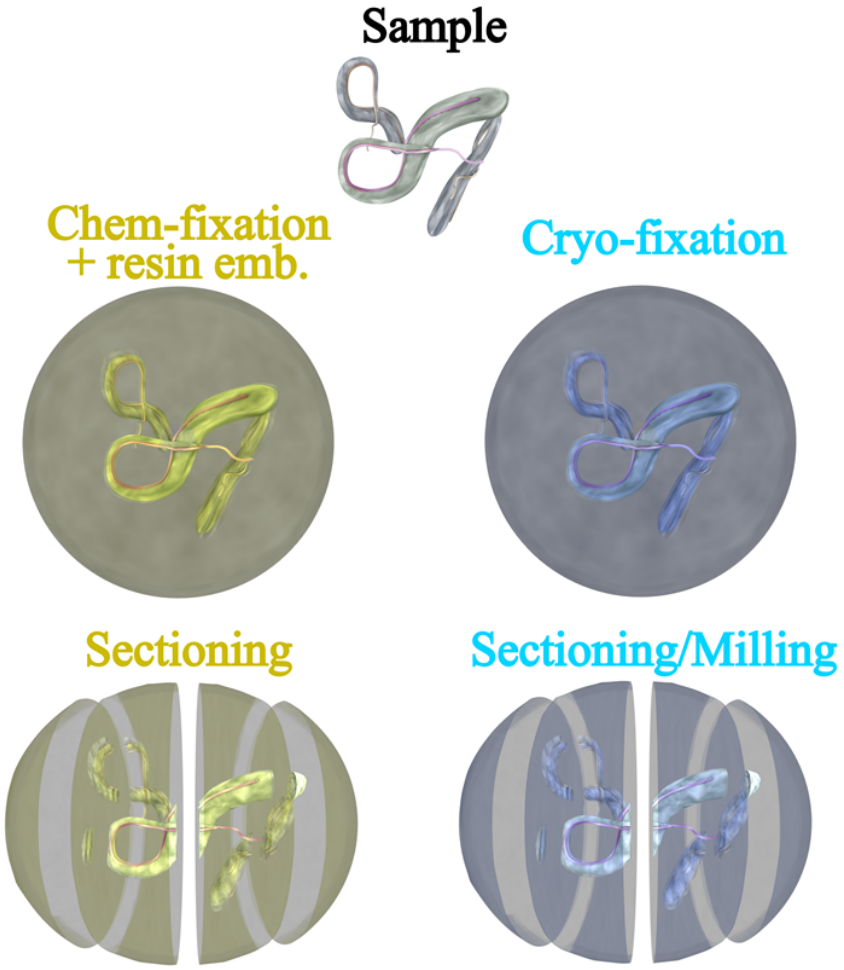

Figure 1: ***Sample preparation methods for parasitology samples suitable for scanning transmission electron microscopy.*** The sample (top), can be either chemically-fixed and resin-embedded (top-left) or cryo-fixed (top-right). The resin-embedding step generates a sizeable resin block several millimetre-thick which must be thinned-down before being imaged at the electron microscope (bottom-left). Cryo-fixed samples which are thin enough to be imaged directly at the electron microscope are usually cryo-fixed using plunge-freezing. But if they are too thick they must be frozen using high-pressure freezing which generates an ice block several hundreds of micrometre-thick which must be thinned-down before being imaged at the electron microscope (bottom-right). For each type of prepared sample, 2D or 3D structural information can be recovered, it only depends on the imaging method used.

One of the main limitations of TEM is the thickness of the samples that can be observed with the typical acceleration voltage of up to 300kV, which is about 300 nm. Therefore, biological samples are typically embedded in resin and sliced into ultrathin sections of less than 100 nm. STEM is an alternative to TEM[3]. STEM allows to image thicker samples than TEM, in particular thicker resin sections[4]. This can be advantageous as it requires the observation of fewer sections for the same sample size. It should be notated that in TEM not the original structures are observed but heavy-metals binding to proteins, lipids and other cellular components. In addition, due to fixation, dehydration and resin embedding, structures are often denatured. This limits access to high-resolution structural information required for accurate studies of the intricate and

fragile cellular structures.

In cryo-electron microscopy, the sample is rapidly cooled down and fixed under cryogenic conditions in a liquid cryogenic fluid (e.g. liquid ethane) (Fig. 1, top-right)[5]. Rapid freezing is required to prevent the formation of ice crystals inside and outside the cells which can be deleterious for the sample integrity and affect the observation under the electron microscope. Samples that are thin enough (< 2-3 µm) such as single-cell organisms can be cryo-fixed directly on an electron microscopy grid using plunge-freezing in liquid ethane cooled-down by liquid nitrogen[6]. Thicker samples including unicellular or multicellular organisms are preferably frozen under high-pressure (~2000 bars) at liquid nitrogen temperature[7]. As no fixative is used and samples remain hydrated, cryo-electron microscopy is the method of choice to study samples in their native state. Yet, this does not lift the thickness requirements of TEM. This is the reason why thick cryo-fixed cells are thinned-down using cryo-sectioning[8] or cryo-focused ion beam (FIB) milling[9] (Fig. 1, bottom-right). These sections/lamellae can be observed either using cryo-TEM or cryo-TEM tomography (cryo-TET)[10]. Combined with averaging computational methods known as sub-tomogram averaging, 3D maps of proteins can be generated *in-situ* at sub-nanometre resolution[11,12].

Cryo-STET was first developed in 2014 at the Weizmann Institute of Science[13]. This pioneering work represented a great step forward as it allows the observation of micrometre-thick samples in their native state by combining STEM and cryo-conditions[14,15]. In 2020, cryo-STET was used to characterise the 3D organisation of the flagellar attachment zone staples in *Trypanosoma brucei* [16]. Because the method is relatively new and is likely to be further improved, the potential of cryo-STET is important, especially in the field of parasitology as the thickness of samples studied fits particularly well within the method capacities and limitations.

The main goal of this review is to familiarise the parasitology readership with the basis of STEM imaging in 2D and 3D workflows. Several applications are presented to outline what can be achieved with the STEM methods. Then, the latest developments and applications in cryo-STET are presented. This overview should provide the readers with a good sense of how they could potentially benefit from using STEM methods.

2D scanning transmission electron microscopy approaches for parasitology

STEM principle & applications

Compared to TEM which uses a spread electron beam, STEM uses a focused electron beam forming a probe[3] which can reach sub-nanometre diameter. This probe is scanned at the specimen level and the transmitted electrons are collected by different post-specimen detectors. Depending on the angle at which electrons have been scattered after their interaction with the sample, electrons are recorded by either bright field (BF), annular dark field (ADF), or high angle annular dark field detectors (HAADF) (Fig. 2). Electrons that do not interact with the sample are not scattered and are collected by the BF detector. Electrons interacting inelastically with the sample (interaction with the electron cloud) are scattered at relatively small angles and are typically collected by the ADF detector. Finally, electrons that interact with the atomic nucleus undergo a scattering at high angle and are collected by the HAADF detector. It is important to note that an electron that went through multiple inelastic scattering has some probability to exit the sample at high angle and then be detected by the HAADF. However, this multiple successive inelastic scattering can only exist in samples with a thickness equal to several times the inelastic mean free path of the electron (i.e., biological samples which are thicker than 0.5 µm). The distance between the specimen and the detectors is called the camera length. It can be virtually modified using lenses of the microscope, thus allowing to vary the collection angles of the different detectors. Inelastic scattering can be discarded by choosing the right camera length and generating images based solely on electrons collected by the BF detector. This method is referred to as STEM BF, which is the mode that will be mainly presented in this review.

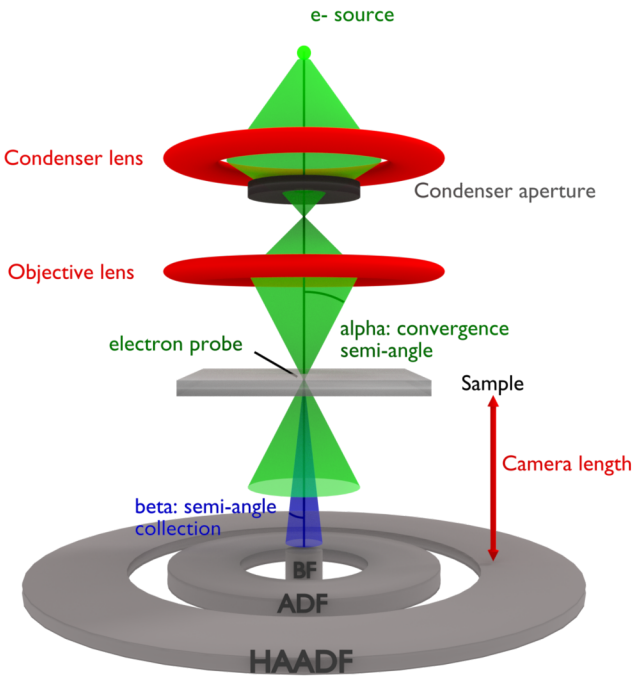

Figure 2: Schematics of the electron beam optical path in STEM. The beam is focused at the sample level, forming a probe that is scanned over the sample in a raster. The diameter of the probe (d) is determined by the convergence semi-angle (α) and the wavelength of the electrons (λ) using the equation $d = \lambda/\alpha$. The depth of field (Δz) is dependent on the convergence semi-angle (α) and the wavelength of the electrons (λ) using the equation $\Delta z = 1.77\ \lambda/\alpha^2$. The camera length value can be modified to change the collection angles of the different detectors (there is a unique camera length for all the detectors).

In STEM, each horizontal line of the image is built point per point. The electron beam follows a raster scanning. To generate each pixel of the line, the number of electrons collected on the detector (BF, ADF or HAADF) is integrated at regular time intervals. The time interval is set by the experimenter and is called the dwell time, typically ranging between 1 and 4 µs in STEM of biological samples. In STEM, the pixel values are generated using amplitude contrast, which is proportional to the mass of the atoms. When the electron beam crosses light elements a great number of electrons pass through the sample without interaction and are collected by the BF detector. Conversely, when the electron beam crosses heavy elements, only a limited number of electrons pass through without interaction as most of these electrons are scattered away from the optical axis and are collected by the ADF or HAADF detector. The geometry of the beam (i.e., its convergence angle) determines the size of the probe and its depth of field. The smaller the convergence angle, the bigger the diameter of the probe. Moreover, as the depth of field is inversely proportional to the probe diameter, the smaller the convergence angle the greater the depth of field[17]. Thus, the size of the probe has a direct implication on the achievable resolution and must be matched with the image pixel size to avoid over- or under-sampling the specimen.

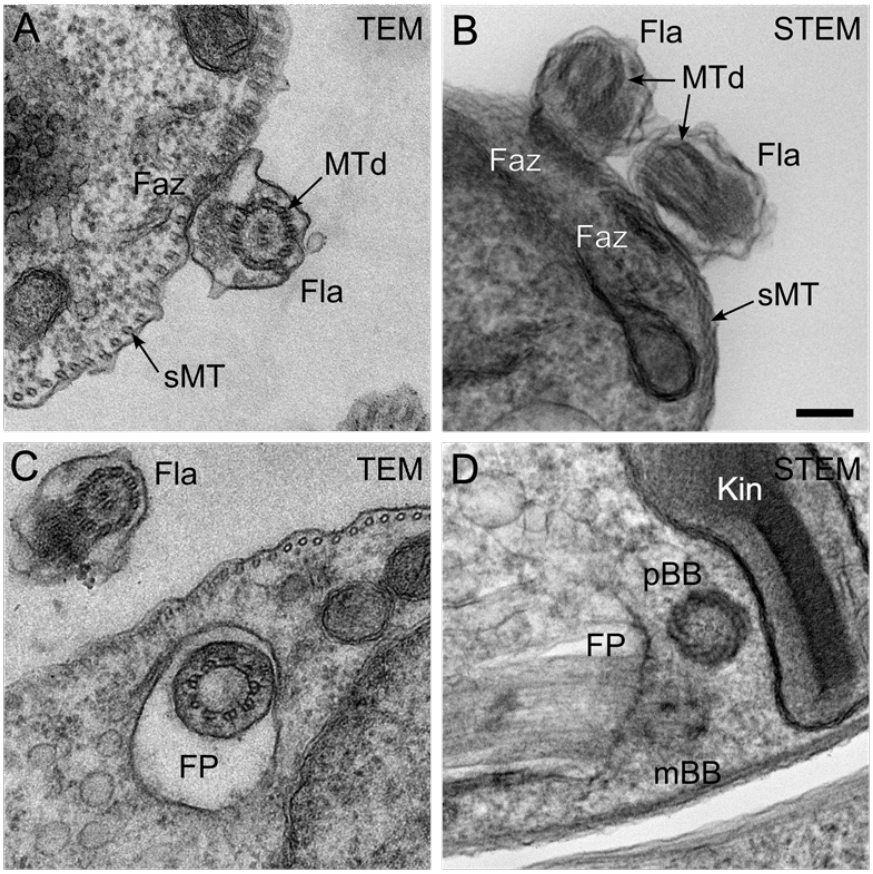

Figure 3: ***TEM and STEM images of resin-embedded sample sections.*** A and B) Respectively TEM and STEM images of extracellular flagellum (Fla) portions and flagellum attachment zones (Faz). The position of microtubules doublets (MTd) and sub-pellicular microtubules (sMT) is indicated. C and D) Respectively TEM and STEM images of *T. brucei*posterior intracellular organisation showing the kinetoplast (Kin), the flagellar pocket (FP) and the mature- and pro-basal bodies (mBB and pBB). The sections observed in TEM are 100 nm thick, whereas the sections observed in STEM are 500 nm thick. BF STEM images were collected on a JEOL 2200FS. Scale bar is 200 nm.

STEM can be used to image thick resin sections of biological samples[18]. Examples showing the differences between TEM and STEM images are presented in Figure 3. Thanks to the use of heavy atom contrasting agents during sample preparation, the contrast of resin section images in STEM is particularly high, even when thick sections are imaged. This is due to the substantial amplitude contrast of heavy atoms. In STEM of thick resin sections, the resin areas have a more homogeneous texture compared to TEM on thin resin sections. In the TEM image (Fig. 3A), the densities of the microtubules (sub-pellicular and axonemal ones) appear shorter, and the details are sharp because it is a projection of a thin section. In the STEM image (Fig. 3B), the microtubules appear longer as a thicker section is imaged. This demonstrates that STEM allows obtaining information over a greater depth compared to conventional thin resin sections used in TEM. In STEM, it is possible to study the kinetoplast, the mature- and pro-basal bodies and a large portion of the flagellum inside the flagellar pocket all at once (Fig. 3D). Being able to observe an organelle as thick as the flagellum over its entire depth, without the need to cut or thin it down, offers the possibility to better understand how the organelle and its constituents are organised. Since many structural details can be observed at once, it allows measuring the dimensions of the organelle components and their distances with much more accuracy than what would be possible using a collection of serial resin sections. Indeed, during

cutting, i) a thin amount of matter is lost between consecutively sliced sections and ii) accurate registration of serial sections is not trivial and prone to measurement errors. In a previous work, STEM of thick resin sections allowed to build the first 3D organisational map of the flagellar pocket in *T. brucei* [19]. Using thicker sections can also be advantageous in observation and/or counting of gold particles in gold-immunolabelled resin sections as it increases statistical measurements.

STEM-in-SEM principle & applications

STEM-in-SEM consists in using a scanning electron microscope (SEM) to obtain images similar to those obtained in a TEM. Because it is based on the use of low voltages (5 to 30 kV instead of $>$ 100 kV used in TEM) it is also known as "low voltage STEM". In SEM, transmitted electrons are typically not collected because the design of the microscope does not allow it since the original purpose of a SEM is to collect backscattered and secondary electrons. The STEM-in-SEM approach was initially proposed in 1972 by designing a tailored SEM stage[20] to obtain transmission images on material sciences specimens. Evolution in the design of the specimen holder allowed to perform DF STEM-in-SEM imaging[21]. These new specimen holders were used in biology to study the internalisation of gold-nanoparticles in bivalve tissues in Spurr resin sections up to 400 nm-thick[22] and the structure of myoblasts in 400 nm-thick EPON sections[23]. These works demonstrate the potential of STEM-in-SEM for the observation of eukaryotic cells and tissues. Allowing the observation of semi-thin sections ($<$ 400 nm) removes the need for ultrathin sections ($<$ 100 nm) which simplifies the ultramicrotomy process to access subcellular structures.

To present more examples of the STEM-in-SEM method, we illustrate the capability of this technic to resolve subcellular details on another sample in Figure 4. In these 100 nm-thick resin sections, fine details can be observed. Organelles such as the Golgi apparatus (Fig. 4A) or viral factories (Fig. 4B) can be clearly identified. Therefore, STEM-in-SEM could be an interesting alternative to the more conventional TEM for histology, cell biology, and basic structural biology.

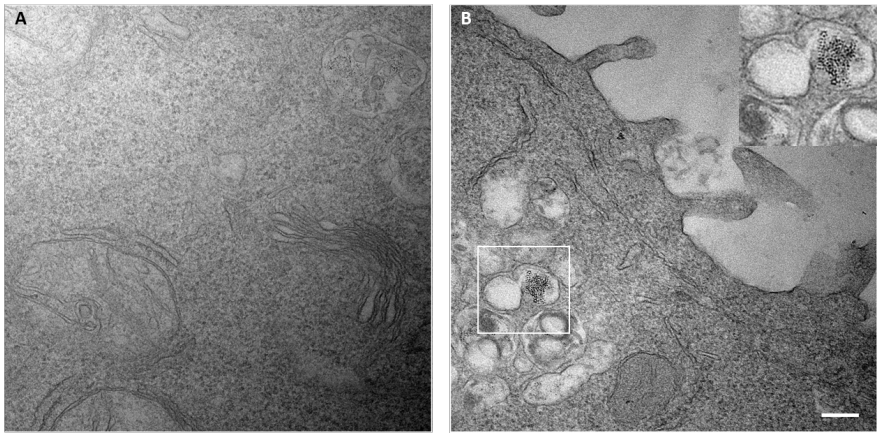

Figure 4: ***STEM-in-SEM images of cell subcellular structures.*** A) Overall view of cytoplasm showing a Golgi apparatus (G) and some mitochondria in the bottom left corner. B) Type A virus infected cell showing a viral factory (box and insert). Samples were EPON resin-embedded and sections were cut to a 100 nm nominal thickness. Observation performed on a JEOL IT800 at working distance 6 mm and 8 kV. Scale bar is 200 nm.

Cryo-STEM principle & applications As introduced above, cryo-STEM combines the benefits of STEM (amplitude contrast and potential to observe thick specimens) and cryo-methods (hydrated specimen in its native state). A cryo-STEM advantage over cryo-TEM is the delayed apparition of radiation damages caused by the electron beam[13]. This is an advantage, especially if multiple images are collected as it is the case in tomography workflows. Cryo-STEM even enables chemical imaging, allowing the study of metal distribution

in proteins such as the distribution of Fe and Zn in ferritin[24]. This has the potential to study the atomic content of specimen using compositional contrast[25]. In summary, cryo-STEM is a very interesting alternative to conventional cryo-TEM for the study of biological samples and, as above-mentioned, it is best adapted to study thick samples. An example of the contrast increase in cryo-STEM is presented in Figure 5, it focuses on the observation of nucleic acids encapsulated in lipid nanoparticles (LNPs) and frozen in presence of 10% sugars (excipients used in pharmaceutical products). In conventional cryo-TEM the contrast is low because of the similar chemical composition of sugars (H, C, O) and nucleic acids-LNPs (H, C, O, P) (Fig. 5A). The use of STEM increases the contrast even in presence of sugars (Fig. 5B). Thus, cryo-STEM helps and allows the observation of different types of organic materials (here sugars and nucleic acid LNPs). This example on LNPs can be extended to larger specimens such as bits of cells thin enough to allow cryo-STEM imaging. Indeed, in the literature, cryo-STEM has been used on different types of eukaryotic cells of varying thickness[14,15].

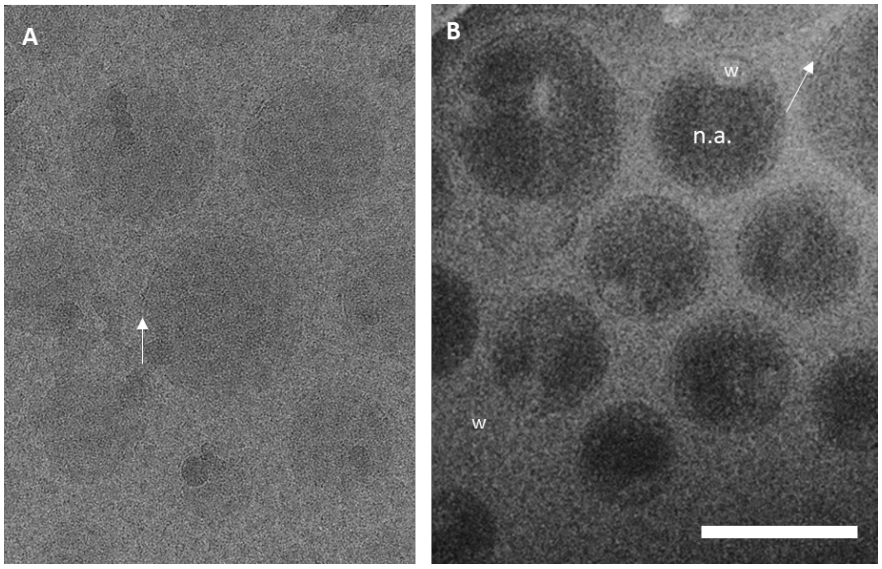

Figure 5: ***Conventional cryo-TEM and cryo-STEM images acquired on the same grid of nucleic acid LNPs on a drug product with 10% sugars.*** A) Conventional cryo-TEM image. B) Cryo-STEM image showing in addition to lipid bilayer, the phase segregation between nucleic acid (n.a.) and water (w) in background vitreous ice and within LNPs. Arrows point at lipid bilayers of LNP. Images were acquired on a Glacios microscope operated at 200KV using a Falcon 4 camera for the conventional cryo-TEM and a Panther STEM detector for the cryo-STEM image.

Because the size of the samples that cryo-STET can investigate perfectly matches the dimensions of numerous unicellular parasites, this method has the potential to make great progress in the unravelling of the complex parasite structure which could help better understand how these cells infect their hosts.

3D scanning transmission electron microscopy approaches for parasitology

Images produced in scanning transmission electron microscopy and in conventional TEM contain structural information of the inside of the object of interest because they are projection images, as opposed to surface images. Projection images can be combined to reconstruct biological objects by computational approaches thus providing access to the 3D structure. When projection images are acquired by tilting the sample around a single axis the computational approach is called tomography[26].

STET principle & applications

Historically, STEM was mostly used in the field of material sciences, even though there were some early uses

of the technique to measure the amino acids content of proteins, thanks to the atomic mass sensitivity of the method[27,28]. In biology, STEM became increasingly popular when the community realised that it could be used to study thick sections of cells embedded in resin[4,17,29,30]. STET of biological samples was then developed to explore cellular and sub-cellular structures of samples embedded in thick resin sections[19,31].

In STET, the sample is tilted at different angles inside the electron microscope and, for each tilt angle an image is collected. In the microscope, the sample cannot be tilted up to ±90° because its apparent thickness would be virtually infinite (at this angle the electrons would have to traverse the whole diameter of the grid). Therefore, the angular collection is incomplete. In the Fourier space, this creates a wedge (called the missing-wedge) which does not contain any information[32]. A typical tilt range is between -60° to +60°, using 2° or 3° increments, but some studies collect images with tilts up to ±70°. Collecting images at higher tilt angles can be useful to fill in and reduce the missing-wedge. During the experiment, the sample must be tracked so that the same field of view is imaged during the whole data collection and focusing must be performed to avoid collecting out-of-focus images. It is particularly important in STEM to collect images in focus otherwise they suffer a strong blurriness[32]. This is particularly true if high convergence semi-angles are used (depth of focus limited to a few tens of nm) but can be mitigated by using low convergence semi-angles (depth of focus up to a few microns). After data collection, the 2D projections must be aligned to a common origin, which can be done by using gold beads as fiducial markers or fiducials-free reference mathematical methods. Then, dedicated algorithms are used to reconstruct the 3D volumes using the aligned 2D projections. The details of these steps are out of the scope of this review but can be found in the literature[26].

Resin sections up to 1 µm-thick can be studied using STET. Because the field of view is usually greater than 1 μm^2, the total volume available in a single 3D reconstruction is greater than 1 μm^3, which corresponds to about the volume of small prokaryote, or using parasitology standards, the whole flagellar pocket of a *T. brucei*cell[19]. In comparison, the sample volume usually captured in conventional TEM ranges between 0.1 and 0.3 μm^3 (for 100 and 300 nm-thick resin sections, respectively, and provided that the field-of-view is 1 μm^2).

Early STET works in biology were performed using the ADF detector as it was often employed in material science studies[4,17]. In tomography, the sample is tilted and its apparent thickness increases inversely proportional to the cosine of the tilt angle. This means that at ±60°, the apparent thickness of a sample is twice its nominal thickness. Because of this, multiple inelastic scattering occurs, leading to the undesirable detection of light elements on the ADF or HAADF detector. This, in turn, results in the collection of noisy ADF/HAADF images. For the observation of thick samples, more meaningful images are obtained using the BF detector[29,31].

In parasitology, STET has so far only been used on a limited number of organisms[19,29]. A video article describing the use of STET on *T. brucei* thick sections is also available[33]. In this review, we introduce another case, also involving *T. brucei* . In this example, STET has been performed on a 500 nm-thick resin section of *T. brucei* , showing structural details next to the mature- and pro-basal bodies, between the flagellar pocket and the kinetoplast of the cell (Figure 6). This is the same region as the one shown in Figure 3D. Each image corresponds to a virtual 10 nm-thick slice within the reconstruction and is separated from the next one by a 20 nm-thick gap. The entire pro-basal body is present in this 500 nm-thick section. The microtubule triplets are clearly visible, with microtubules A, B and C well-delineated. The flagellum is slightly tilted inside the reconstruction as we can see it appearing from the top of the image and disappearing from the bottom. It extends from the mature basal body, which is almost fully contained in the resin section. The penultimate image corresponds to the centre of the flagellum as the central pair is visible above the basal plate. The microtubule quartet is visible on the third and fourth images (Fig. 6C and D). The microtubules of the quartet are then directed towards the anterior part of the cell and are visible on the left side of the flagellar pocket membrane in the fifth and sixth images (Fig. 6E and F). On the bottom part of the images, the large kinetoplast is easily recognised thanks to its specific shape and texture. The disk of the kinetoplast DNA is particularly well defined. Other details could be described in this dataset, such as some thin strings connecting the kinetoplast and the mature basal body or the collarette around the flagellum membrane in

the flagellar pocket (Fig. 6F). However, what we want to point out here is the large volume of structural information one can get in using STET on thick resin sections. Using a 200 kV STEM capable electron microscope, 750 nm-thick resin sections can routinely be studied.

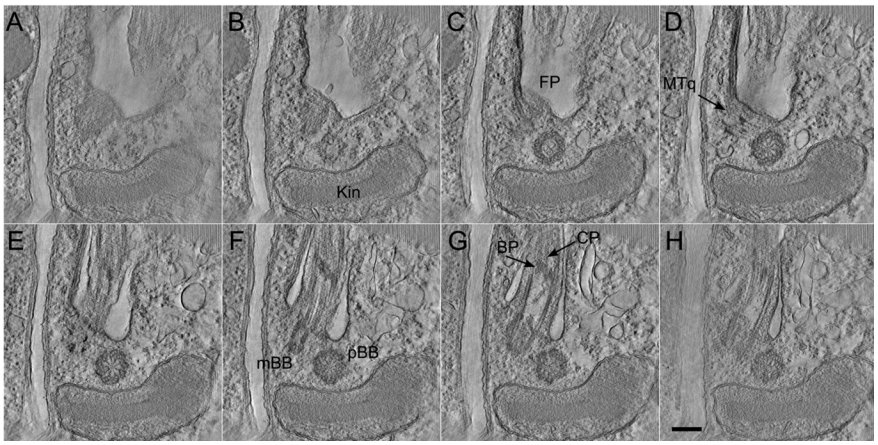

Figure 6: ***STET analysis of a T. brucei cell posterior part.*** A-H) These images are 10 nm thick virtual sections extracted from a STET reconstruction of a 500 nm thick resin section. This volume contains the mature- and pro-basal bodies (mBB and pBB), the kinetoplast (Kin) and a large portion of the flagellar pocket (FP). Other structural elements can be recognized, the microtubule quartet (MTq) and the basal plate (BP) from which the central pair of microtubules (CP) emerges. Scale bar is 200 nm.

Cryo-STET principle & applications

Cryo-STET was developed in 2014 with the pioneering work of Wolf*et al.* [13]. Up to now, less than a handful of laboratories have implemented cryo-STET, which might illustrate the difficulty of setting up the method. However, a recent video-based article explains very well how to perform the data collection[34] hopefully inspiring researchers to use the method and apply it to different biological systems. As with cryo-TEM and cryo-STEM methods, the specimens studied in cryo-STET are cryo-fixed, which protects and maintains the sample native state. Cryo-STET is a 3D imaging method, which can theoretically be used to observe samples thicker than the ones studied in room-temperature STET. The reason is that room-temperature STET observes chemically fixed and heavy metal-stained samples, which then contain atoms heavier than the original organic ones, reducing the electron mean free path and their penetration through matter. In cryo-STET, only typical organic atoms are present (mainly H, C and O), allowing the observation of samples as thick as 1 µm and beyond[35]. Then, in terms of volume of information, cryo-STET exceeds by far what is possible in cryo-TET (by one order in magnitude). Because cryo-STET can observe samples slightly thicker than 1 µm, the exploration of basically any unicellular eukaryotic parasite species becomes possible (e.g. *Trypanosoma sp.* , *Leishmania sp.* and *Toxoplasma sp.).* Yet, as explained above, cryo-STET is not a trivial method. The successful collection of cryo-STET data requires first a correct understanding of the concepts associated with STEM imaging, which differ from those associated with TEM imaging.

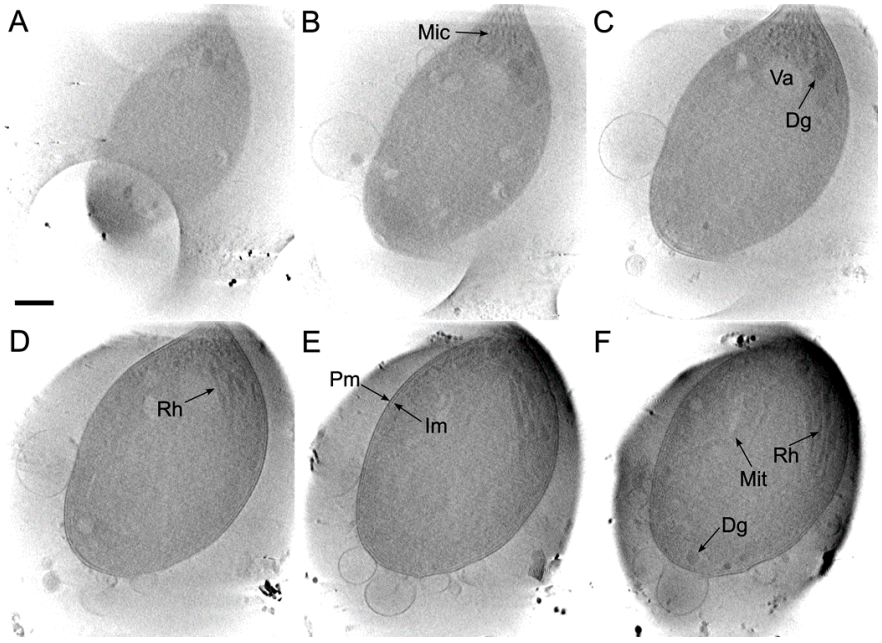

Figure 7: ***Cryo-STET analysis of a T. gondii tachyzoite.*** A-F) These images are 25 nm thick virtual sections extract for a cryo-STET reconstruction of an entire *T. gondii* tachyzoite cell. Several intracellular structures are visible in the reconstruction. At the top, the micronemes (Mic) next to the vacuole (Va) and some dense granules (Dg). Rhoptries (Rh) are clearly identified thanks to their strong contrast, and the mitochondria (Mit) is also visible, yet with lighter contrast. The plasma membrane (Pm) and the internal membrane complex (Im) are resolved at several locations. Scale bar is 500 nm.

Cryo-STET has been used to investigate the 3D structure of various bacterial and eukaryotic cells (including unicellular parasites)[16,36–38]. To present the cryo-STET method, we estimated that the best would be to apply the method on a new type of sample previously unpublished. Figure 7 shows the ultrastructure of a*T. gondii* tachyzoite cell. This cell is one of the thickest cells studied using cryo-STET and is almost 2 µm thick and 3.5 µm long. Such a thickness might represent the current limit for cryo-STET studies. Despite the thickness of this sample, several internal structural elements are clearly visible with a fair amount of details. At the top, the tip of the cell is packed with micronemes (Mic) identified by their typical shape and texture, a vacuole (Va) and some dense granules (Dg) (Fig. 7B and C). In this dataset, the conoid is unfortunately outside of the field of view, it would otherwise be visible above the micronemes. Going down to the other side of the cell, the rhoptries (Rh) are particularly visible thanks to their usual high contrast. Next to the rhoptries, it is possible to spot a long vesicle-like structure slightly darker than the cytoplasm, which likely corresponds to the mitochondria (Mit) (Fig. 7F). At the periphery of the cell, and visible on most of the reconstruction slices, the plasma membrane (Pm) and the internal membrane complex (Im) are resolved. Again, the potential of STET, especially under cryo-conditions, is tremendous compared to what can be achieved in conventional TEM which would have required the use of many sections.

Further applications and future developments in cryo-STET

For many of the samples studied in cryo-STET, they can be directly deposited (or grown) and frozen on cryo-EM grids. This allows the cells to be studied using light and fluorescence microscopy before cryo-fixation. This workflow is referred to as the correlative light and electron microscopy method (also known as CLEM). The correlative study can be performed on the whole sample because the cells do not require cutting before observation at the electron microscope as the thickness requirement of cryo-STET allows it. The cryo-fixation method for such samples is easily performed using plunge-freezing, where the grid is rapidly plunged inside a cryogen (usually ethane) cooled-down at about -175°C by liquid nitrogen. It must be noted

that such samples are the thickest ones that can be properly frozen using plunge-freezing. Interestingly, the thickness limitation of cryo-STET is equivalent to the thickness limitation of plunge-freezing. For thicker samples, plunge-freezing can no longer be used without the formation of ice crystals. These crystals would be deleterious for imaging as they would diffract electrons which would no longer be detected on the BF detector. This means that thicker samples must be frozen at high-pressure. This cryo-fixation method, far more complex than plunge-freezing, involves an equipment which is more expansive than a simple plunge-freezer and generates a thicker layer of vitrified ice which is at least several tens of µm thick. It is possible to image this slab of frozen sample using a cryo-FIB SEM. But if cryo-STET is required (e.g. for resolution purposes since cryo-STET offers higher resolutions compared to cryo-FIB SEM), then a cryo-lamella could be prepared to thin-down the thick slab of ice down to 1 µm using a cryo-FIB. This process adds even more complexity to the realisation of the experiment.

The examples presented in this review all used BF STEM, yet this is not the only modality available. As previously briefly presented, ADF and HAADF imaging can inform about the presence of atoms heavier than the most abundant organic atoms (H, C and O) such as K, Ca, Fe. Another method, differential phase contrast (DPC) has recently been applied in biology[39–41]. This method uses a modified ADF detector which is composed of 4 quadrants, each representing a 90° portion of the full detector. It is then possible to split the electrons arriving on the detector in 4 different populations (top, bottom, left and right) and their analysis allows to retrieve the sample phase information, hence the name of the method. As the application of this method to biological samples is extremely recent, its successful application on thick samples still has to be demonstrated.

Current cryo-STET resolution and sample thickness limits are associated to the electron dose used during the experiment. To achieve high resolutions, the sampling (pixel size) has to be small, however a dense sampling of the specimen mechanically increases the electron dose. To achieve a two-fold resolution increase, the pixel size must be two times smaller, leading in a four-fold increase of the electron dose. Since images are already collected with the maximum electron dose the specimen can sustain, experiments aiming at resolution increases are dose-limited and must deal with the collection of low-dose, low signal-to-noise ratio images. To image thick specimens in BF STEM, the electron dose must be high as thick samples scatter electrons more than thin ones. Thus, there is a limit in the maximum achievable sample thickness which is when the electron dose becomes too high and starts generating visual damages to the sample. Sparse imaging has the potential to tackle both limitations at once. Sparse imaging consists in the collection of a limited number of pixels (as opposed to collecting the whole image pixels), which mechanically reduces the electron dose applied to the area of interest. This method is possible in STEM as the point-to-point image generation allows it. The uncollected missing pixels must be somehow reconstructed to generate the image of the area of interest. This can be performed using inpainting algorithms[42]. The sparse imaging + inpainting reconstruction workflow can be applied to room temperature and cryo-samples in 2D and 3D experiments[43,44]. By reducing the electron dose, it opens the way to higher resolution or thicker sample studies.

Conclusion

Although STEM is mainly used in materials sciences, there are many applications in biology that would benefit from STEM imaging. However, until now very few groups have explored the potential of STEM imaging. The aim of this review was to describe the STEM methods used in parasitology and other fields. We have demonstrated using several examples that STEM and cryo-STEM are superior to TEM and cryo-TEM under specific conditions. STEM methods perform remarkably well with thick samples. Since parasites are thick samples, STEM imaging can be particularly beneficial. Cryo-STET in particular, is a perfect fit for the study of micrometre thick samples as they can simply be deposited or grown directly on electron microscopy grids, which makes sample preparation protocol easier and faster to execute.

Another important detail of STEM imaging is its relative low cost compared to the acquisition of a TEM-related equipment (direct electron detector, energy filter). Electron microscopes used in biology are more and more often equipped with STEM detectors. Because STEM is now being used for more than a decade, there

are many tools available, from data collection to image analysis. The transition from room temperature to cryo-conditions will be motivated by the possibility to i) recover native structural information and ii) perform CLEM experiments. These events are a huge benefit for the scientists who would like to ride on the STEM wave and want to join cutting-edge technologies.

Figure caption

Figure 1: ***Current approaches in scanning transmission electron microscopy suitable for parasitology.*** The sample (top), can be either chemically-fixed and resin-embedded (top-left) or cryo-fixed (top-right). The resin-embedding step generates a thick block which must be thinned-down before being imaged at the electron microscope (bottom-left). Cryo-fixed samples can be thin enough (plunge-frozen) to be imaged in cryo-STEM. But if they are too thick (high-pressure freezing) they must be cut.

Figure 2: Schematics of the electron beam optical path in STEM. The beam is focused at the sample level, forming a probe that is scanned over the sample in a raster. The size of the probe is determined by the convergence semi-angle ($d = \lambda/\alpha$). The depth of field is also dependent on the convergence semi-angle ($\Delta z = 1.77\ \lambda/\alpha 2$). The camera length value can be modified to change the collection angles of the different detectors (a unique camera length for all the detectors).

Figure 3: ***TEM and STEM images of resin-embedded sample sections.*** A and B) Respectively TEM and STEM images of extracellular flagellum (Fla) portions and flagellum attachment zones (Faz). The position of microtubules doublets (MTd) and sub-pellicular microtubules (sMT) is indicated. C and D) Respectively TEM and STEM images of*T. brucei* posterior intracellular organisation showing the kinetoplast (Kin), the flagellar pocket (FP) and the mature- and pro-basal bodies (mBB and pBB). The sections observed in TEM are 100 nm thick, whereas the sections observed in STEM are 500 nm thick. Scale bar is 200 nm.

Figure 4: ***STEM-in-SEM images of cell subcellular structures.*** A) Overall view of cytoplasm showing a Golgi apparatus (G) and some mitochondria in the bottom left corner. B) Type A virus infected cell showing a viral factory (box and insert). Samples were EPON resin-embedded and sections were cut to a 100 nm nominal thickness. Observation performed on a JEOL IT800 at working distance 6 mm and 8 kV. Scale bar is 200 nm.

Figure 5: ***Conventional cryo-TEM and cryo-STEM images acquired on the same grid of nucleic acid LNPs on a drug product with 10% sugars.*** A) Conventional cryo-TEM image. B) Cryo-STEM image showing in addition to lipid bilayer, the phase segregation between nucleic acid (n.a.) and water (w) in background vitreous ice and within LNPs. Arrows point at lipid bilayers of LNP. Images were acquired on a Glacios microscope operated at 200KV using a Falcon 4 camera for the conventional cryo-TEM and a Panther STEM detector for the cryo-STEM image.

Figure 6: ***STET analysis of a T. brucei cell posterior part.*** A-H) These images are 10 nm thick virtual sections extracted from a STET reconstruction of a 500 nm thick resin section. This volume contains the mature- and pro-basal bodies (mBB and pBB), the kinetoplast (Kin) and a large portion of the flagellar pocket (FP). Other structural elements can be recognized, the microtubule quartet (MTq) and the basal plate (BP) from which the central pair of microtubules (CP) emerges. Scale bar is 200 nm.

Figure 7: ***Cryo-STET analysis of a T. gondii tachyzoite.***A-F) These images are 25 nm thick virtual sections extract for a cryo-STET reconstruction of an entire *T. gondii* tachyzoite cell. Several intracellular structures are visible in the reconstruction. At the top, the micronemes (Mic) next to the vacuole (Va) and some dense granules (Dg). Rhoptries (Rh) are clearly identified thanks to their strong contrast, and the mitochondria (Mit) is also visible, yet with lighter contrast. The plasma membrane (Pm) and the internal membrane complex (Im) are resolved at several locations. Scale bar is 500 nm.

Acknowledgements

ST would like to acknowledge S. Perrot and P. Bastin from Institut Pasteur, Paris, France for providing the *T. brucei* sample and T. Mouveaux and M. Gissot from Institut Pasteur Lille, France for providing the

T. gondii sample. The authors would like to acknowledge Jean-Sébastien Bolduc from Sanofi for editorial assistance.

References

1. Cooper, C., Thompson, R. C. A. & Clode, P. L. Investigating parasites in three dimensions: trends in volume microscopy. *Trends in Parasitology* **0** , (2023).

2. Harrison, F. & Corliss, J. *Microscopic Anatomy of Invertebrates, Volume 1: Protozoa* . (Wiley-Liss, New-York, 1991).

3. Nellist, P. D. The Principles of STEM Imaging. in *Scanning Transmission Electron Microscopy* (eds. Pennycook, S. J. & Nellist, P. D.) 91–115 (Springer New York, 2011). doi:10.1007/978-1-4419-7200-2_2.

4. Aoyama, K., Takagi, T., Hirase, A. & Miyazawa, A. STEM tomography for thick biological specimens. *Ultramicroscopy* **109** , 70–80 (2008).

5. Dubochet, J. & McDowall, A. w. Vitrification of Pure Water for Electron Microscopy. *Journal of Microscopy* **124** , 3–4 (1981).

6. Dubochet, J. *et al.* Cryo-electron microscopy of vitrified specimens. *Q Rev Biophys* **21** , 129–228 (1988).

7. Dahl, R. & Staehelin, L. A. High-pressure freezing for the preservation of biological structure: Theory and practice. *Journal of Electron Microscopy Technique* **13** , 165–174 (1989).

8. Al-Amoudi, A. *et al.* Cryo-electron microscopy of vitreous sections. *EMBO J* **23** , 3583–3588 (2004).

9. Mahamid, J. *et al.* A focused ion beam milling and lift-out approach for site-specific preparation of frozen-hydrated lamellas from multicellular organisms. *Journal of Structural Biology***192** , 262–269 (2015).

10. Höög, J. L., Bouchet-Marquis, C., McIntosh, J. R., Hoenger, A. & Gull, K. Cryo-electron tomography and 3-D analysis of the intact flagellum in Trypanosoma brucei. *Journal of Structural Biology***178** , 189–198 (2012).

11. Koyfman, A. Y. *et al.* Structure of Trypanosoma brucei flagellum accounts for its bihelical motion. *Proceedings of the National Academy of Sciences* **108** , 11105–11108 (2011).

12. Zhang, J. *et al.* Structure of the trypanosome paraflagellar rod and insights into non-planar motility of eukaryotic cells.*Cell Discov* **7** , 1–17 (2021).

13. Wolf, S. G., Houben, L. & Elbaum, M. Cryo-scanning transmission electron tomography of vitrified cells. *Nat Methods* **11** , 423–428 (2014).

14. Wolf, S. G. & Elbaum, M. CryoSTEM tomography in biology. in*Methods in Cell Biology* vol. 152 197–215 (Elsevier, 2019).

15. Wolf, S. G., Shimoni, E., Elbaum, M. & Houben, L. STEM Tomography in Biology. in *Cellular Imaging* (ed. Hanssen, E.) 33–60 (Springer International Publishing, 2018). doi:10.1007/978-3-319-68997-5_2.

16. Trépout, S. In situ structural analysis of the flagellum attachment zone in Trypanosoma brucei using cryo-scanning transmission electron tomography. *Journal of Structural Biology: X* **4** , 100033 (2020).

17. Biskupek, J., Leschner, J., Walther, P. & Kaiser, U. Optimization of STEM tomography acquisition — A comparison of convergent beam and parallel beam STEM tomography. *Ultramicroscopy* **110** , 1231–1237 (2010).

18. Trepout, S., Messaoudi, C., Perrot, S., Bastin, P. & Marco, S. Scanning transmission electron microscopy through-focal tilt-series on biological specimens. *Micron* **77** , 9–15 (2015).

19. Trépout, S., Tassin, A.-M., Marco, S. & Bastin, P. STEM tomography analysis of the trypanosome transition zone. *Journal of Structural Biology* **202** , 51–60 (2018).

20. Woolf, R. J., Joy, D. C. & Tansley, D. W. A transmission stage for the scanning electron microscope. *J. Phys. E: Sci. Instrum.***5** , 230 (1972).

21. Patel, B. & Watanabe, M. An inexpensive approach for bright-field and dark-field imaging by scanning transmission electron microscopy in scanning electron microscopy. *Microsc Microanal* **20** , 124–132 (2014).

22. García-Negrete, C. A., Haro, M. C. J. de, Blasco, J., Soto, M. & Fernández, A. STEM-in-SEM high resolution imaging of gold nanoparticles and bivalve tissues in bioaccumulation experiments. *Analyst***140** , 3082–3089 (2015).

23. Leite, P. E. C. *et al.* Gold nanoparticles do not induce myotube cytotoxicity but increase the susceptibility to cell death. *Toxicology in Vitro* **29** , 819–827 (2015).

24. Elad, N., Bellapadrona, G., Houben, L., Sagi, I. & Elbaum, M. Detection of isolated protein-bound metal ions by single-particle cryo-STEM. *Proc. Natl. Acad. Sci. U.S.A.* **114** , 11139–11144 (2017).

25. Elbaum, M., Seifer, S., Houben, L., Wolf, S. G. & Rez, P. Toward Compositional Contrast by Cryo-STEM. *Acc. Chem. Res.* **54** , 3621–3631 (2021).

26. Frank, J. *Electron Tomography* . (Springer US, 1992). doi:10.1007/978-1-4757-2163-8.

27. Engel, A. Molecular weight determination by scanning transmission electron microscopy. *Ultramicroscopy* **3** , 273–281 (1978).

28. Engel, A. & Colliex, C. Application of scanning transmission electron microscopy to the study of biological structure. *Curr Opin Biotechnol* **4** , 403–411 (1993).

29. Hohmann-Marriott, M. F. *et al.* Nanoscale 3D cellular imaging by axial scanning transmission electron tomography. *Nat Methods***6** , 729–731 (2009).

30. Midgley, P. A. & Weyland, M. STEM Tomography. in *Scanning Transmission Electron Microscopy* (eds. Pennycook, S. J. & Nellist, P. D.) 353–392 (Springer New York, 2011). doi:10.1007/978-1-4419-7200-2_8.

31. Walther, P. *et al.* STEM tomography of high-pressure frozen and freeze-substituted cells: a comparison of image stacks obtained at 200 kV or 300 kV. *Histochem Cell Biol* **150** , 545–556 (2018).

32. Rachel, R. Dual-axis STEM tomography at 200 kV: setup, performance, limitations. 40.

33. Trépout, S., Bastin, P. & Marco, S. Preparation and Observation of Thick Biological Samples by Scanning Transmission Electron Tomography. *JoVE* 55215 (2017) doi:10.3791/55215.

34. Kirchweger, P., Mullick, D., Wolf, S. & Elbaum, M. Visualization of Organelles In Situ by Cryo-STEM Tomography. https://app.jove.com/t/65052/visualization-of-organelles-in-situ-by-cryo-stem-tomography (2023).

35. Rez, P., Larsen, T. & Elbaum, M. Exploring the theoretical basis and limitations of cryo-STEM tomography for thick biological specimens. *Journal of Structural Biology* **196** , 466–478 (2016).

36. Adar-Levor, S., Goliand, I., Elbaum, M. & Elia, N. Studying the Spatial Organization of ESCRTs in Cytokinetic Abscission Using the High-Resolution Imaging Techniques SIM and Cryo-SXT. in *The ESCRT Complexes* (eds. Culetto, E. & Legouis, R.) vol. 1998 129–148 (Springer New York, 2019).

37. Kirchenbuechler, D. *et al.* Cryo-STEM Tomography of Intact Vitrified Fibroblasts. *AIMS Biophysics* **2** , 259–273 (2015).

38. Wolf, S. G. *et al.* 3D visualization of mitochondrial solid-phase calcium stores in whole cells. *eLife* **6** , e29929 (2017).

39. Seifer, S., Houben, L. & Elbaum, M. Flexible STEM with Simultaneous Phase and Depth Contrast. *Microsc Microanal* **27** , 1476–1487 (2021).

40. Lazić, I. *et al.* Single-particle cryo-EM structures from iDPC–STEM at near-atomic resolution. *Nat Methods* (2022) doi:10.1038/s41592-022-01586-0.

41. Li, X. *et al.* Imaging biological samples by integrated differential phase contrast (iDPC) STEM technique. *Journal of Structural Biology* **214** , 107837 (2022).

42. Wang, G., Garcia, D., Liu, Y., de Jeu, R. & Johannes Dolman, A. A three-dimensional gap filling method for large geophysical datasets: Application to global satellite soil moisture observations. *Environmental Modelling & Software* **30** , 139–142 (2012).

43. Trépout, S. Tomographic Collection of Block-Based Sparse STEM Images: Practical Implementation and Impact on the Quality of the 3D Reconstructed Volume. *Materials* **12** , 2281 (2019).

44. Cossa, A., Arluison, V. & Trépout, S. Sparse cryo-STEM tomography for biological samples. *Microsc Microanal* **27** , 3028–3030 (2021).